Chapter5

$BiVO_4$–Reduce Graphene Oxide Nanocomposite based Supercapacitor with Excellent Cycle Stability

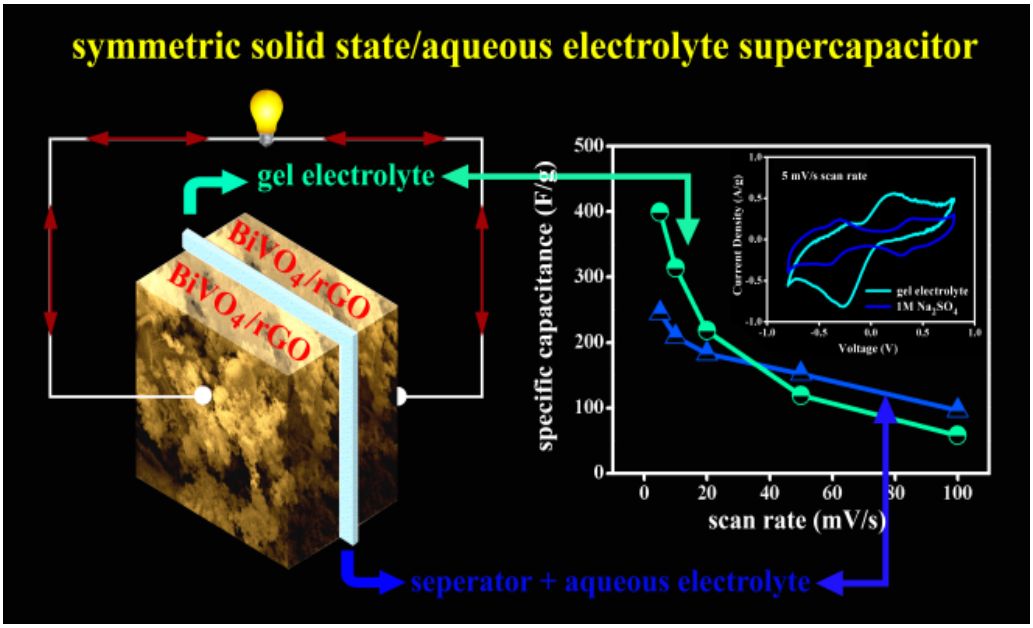

Work presented in this chapter has been published in:

New J. Chem., 2018, 42, 10161-10166

Shibsankar Dutta, Shreyasi Pal, Sukanta De

5.1. Introduction

In this chapter we demonstrate the synthesis of $BiVO_4$/rGO hybrid nanostructure by a simple hydrothermal method. Symmetric cell based on this hybrid nanostructure was fabricated and tested electrochemical properties in both PVA/H_2SO_4 gel and aqueous Na_2SO_4 electrolyte. $BiVO_4$/rGO hybrid based symmetric supercapacitor exhibits better performance in solid electrolyte with high specific capacitance of 400 F/g at 5mV/s and excellent energy density of 35.37 Wh/kg. The as fabricated symmetric supercapacitor shows excellent stability which retains 98% of its initial capacitance after 1000 cycles.

In the last few decades, Compare to the individual transition metal oxides, binary transition metal oxides such as $MnWO_4$,[7] $NiCo_2O_4$,[8] $CoMoO_4$-$NiMoO_4$,[9] $NiMoO_4$,[10] $MnCo_2O_4$,[11] ZnV_2O_4,[12] $LiZnVO_4$,[13] $ZnFe_2O_4$,[14] $CuCo_2O_4$,[15] and $ZnCo_2O_4$[16] grasped enormous attention to the researchers for their excellent electrochemical performance due to their high conductivity and higher electrochemical activity.

It has been already seen that bismuth-based nanostructured materials have caught researcher's great attention due to their applications in semiconductors, catalysts and biomedicine. Among these bismuth family materials, narrow band gaped; bismuth vanadate ($BiVO_4$) has received great attention due to their wide range of applications in ferroelectrics, photocatalytic activity, photochemical solar cells etc.[7-10] To date, crystalline bismuth vanadates has been prepared by a variety of synthesis methods, including solid state reaction, hydrothermal treatment, sonochemistry and metalorganic decomposition and co-precipitation process.[10-13]. Preparation of well crystalline monoclinic $BiVO_4$ can be possible by simple hydrothermal route due to which hydrothermal process is the first choice to the researcher among the different synthesis process. $BiVO_4$ is an electro-active metal oxide which is novel candidate for energy storage applications due to its unique properties. However, $BiVO_4$ suffer from lower electrical conductivity which can be improved by forming a hybrid or composite with conducting materials and for this purpose different porous and conducting carbon materials are the good choice. Khan and his co-worker already reported that 20 Wt% SWCNT based BiVO4 composite electrodes exhibited the specific capacitance value 395 F/g at 2.5 A/g.[14] Patil et al. reported fern like $BiVO_4$/rGO composite obtained specific capacitance 151 F/g under the current density of 0.15 mA/cm^2.[15] Arora and her co-worker reported MoS_2/$BiVO_4$ composites supercapacitor delivered specific capacitance 610 F/g at 1A/g current density.[16]

5.2. Experimental

The $BiVO_4$ nanoparticles were prepared by simple hydrothermal route.[18] In the details synthesis 4.90 g $Bi(NO_3)_3.5H_2O$ was added to the 20 ml 4mol.dm^{-3} HNO_3 solution, whereas 1.85g Na_3VO_4 was added to the 20 ml 2mol.dm^{-3} NaOH solution. Then 0.25 g SDS was added to each the above solutions. After 30 min stirring mixed the as prepared solutions. The pH value of the mixture was then adjusted to 7 adding 2mol.dm^{-3} NaOH solution under vigorous stirring and kept it for another 30 min. Finally precursor solution was transferred into a Teflon-lined stainless steel autoclave and kept it at 200 °C for 90 min. After the autoclave was cooled to room temperature and the precipitate was washed by D.I. water and ethanol several times and kept at 100 °C for 4 h. The time variation of the above experiment was also performed keeping all other parameters same. Henceforth, we designate the samples corresponding to 30 min, 60 min, 90 min and 120 min reaction span as B-30, B-60, B-90 and B-120 respectively. In the present reaction due to the hydrolysis of $Bi(NO_3)_3.5H_2O$, soluble $BiONO_3$ was initially formed which reacted with the VO^{3-} ions provided by Na_3VO_4 at pH ~7 and formed the yellow precipitate of tetragonal $BiVO_4$. In the above reaction pH of the solution was controlled by the NaOH. For the duration of hydrothermal treatment, the formed $BiVO_4$ nuclei were converted to the well crystalline structure of monoclinic $BiVO_4$ nanocrystals. The probable reactions taking place in the BiVO4 formation are shown below

$$\mathbf{Bi(NO_3)_3.5H_2O + HNO_3 + H_2O \rightarrow BiONO_3 + 3HNO_3} \quad \textbf{(1)}$$

$$\mathbf{BiONO_3 + Na_3VO_4 + H_2O \rightarrow BiVO_4 + NaNO_3 + NaOH} \quad \textbf{(2)}$$

For the synthesis of $BiVO_4$/rGO hybrids, graphene oxide (GO) was prepared by modified Hummers method.[17] to prepare different $BiVO_4$/rGO hybrids, different concentration of GO solution (20 mL, 40 mL and 60 mL) with initial concentration (1mg/mL) was added to the above mentioned mixture and kept at hydrothermal reaction at 200 °C for 90 min. Henceforth we denote the $BiVO_4$/rGO samples using 20 mg, 40 mg and 60 mg of GO contents as the BG1, BG2 and BG3.

5.3 Characterizations

Powder X-ray diffraction (XRD) patterns of the as prepared samples were recorded to determine the phase formation and purity using Rigaku-Ultima III X-ray diffractometer with CuKα radiation (λ = 1.5418 Å). Raman spectra were obtained using spectrometer IHR550 and the laser of excitation wavelength 532 nm, The Surface morphology and microstructure of the as prepared materials were characterized by FESEM (HITACHI

S-4800), TEM (JEOL- 2010) and X-ray photoelectron spectroscopy (XPS) of the prepared materials were obtained by SPECS HSA-3500 hemispherical analyzer with monochromatic Mg Kα X-ray source.

5.4. Results and discussion

5.4.1. Structural & morphological analysis:

The micrograph of the sample for a nominal growth time of 30 min (B-30) shows that few undeveloped structures consists with particulate nature start to form (Fig.5.1a). However, for the increase of reaction time no specific shape was formed within 60 min duration (B-60) which is cleared from Fig. 5.1b. For the optimum growth duration of 90 min (sample B-90), well distributed $BiVO_4$ nanoparticles having almost same in shape and size with an average dimension of ~20–30 nm are formed (Fig.5.1c). Further prolonging the reaction span up to 120 min for sample B-120, $BiVO_4$ nanoparticles are agglomerated and attached together to form larger particles of irregular dimensions (Fig.5.1d). Fig.5.2 shows the FESEM images of $BiVO_4$/rGO hybrids revealing the presence of both the $BiVO_4$ nanoparticles and rGO thin sheets. Fig.5.2 shows the FESEM images of $BiVO_4$/rGO hybrids, where the thin sheets of rGO are well wrapped with the $BiVO_4$ (B-90) nanoparticles.

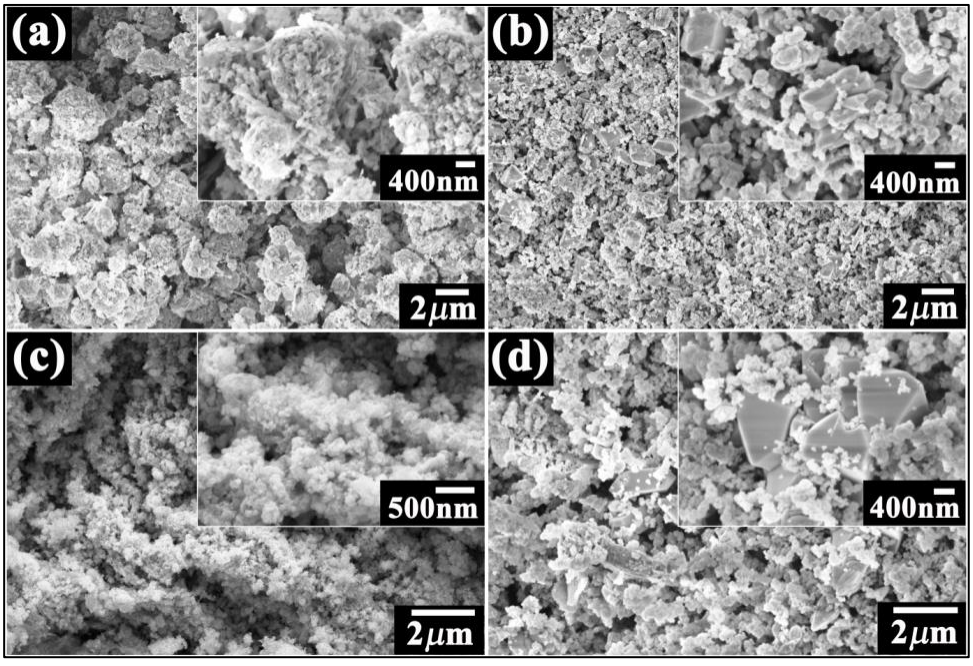

Figure 5.1: FESEM images of (a) B-30, (b) B-60, (c) B-90 and (d) B-120 samples; insets showing their high magnification view.

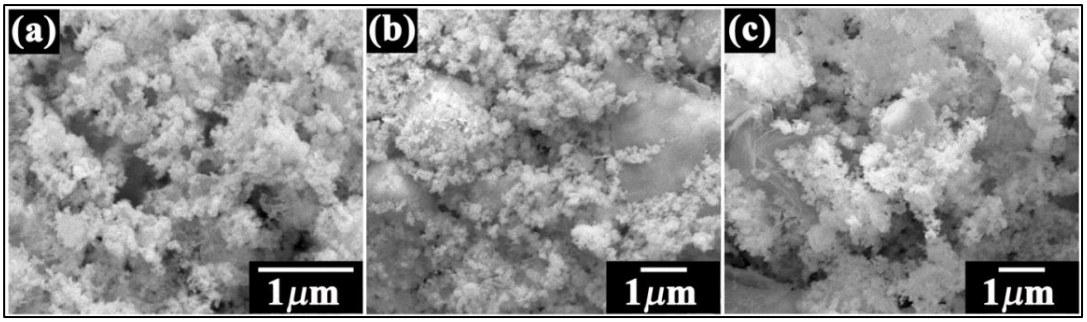

Figure 5.2: FESEM images of (a) BG1, (b) BG2, (c) BG3 samples.

The XRD patterns of all $BiVO_4$ samples that were synthesized under various conditions presented in Fig.5.3(a) also confirm the phase purity of samples. The XRD pattern of the as synthesized $BiVO_4$ indicates the formation of pure phase monoclinic crystal structure of $BiVO_4$ and the peaks could be indexed according to the previously reported data (JCPDS# 014-0688**).**

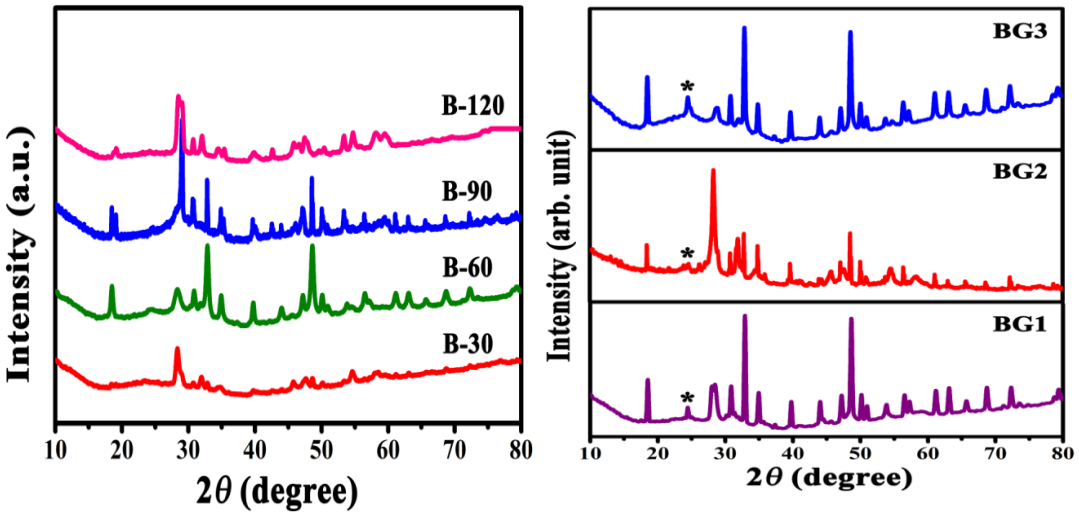

Figure 5.3: XRD pattern of $BiVO_4$ samples synthesized at different reaction time(a), $BiVO_4$/rGO samples with GO concentration variation(b).

In case of $BiVO_4$/rGO hybrids the diffraction peaks (*) correspond to rGO was observed at 2θ~ 25.1º confirms the presence of rGO in the samples (Fig. 5.3 b). Further, FESEM and XRD results reveals that among the all samples B90 and BG2 was well crystalline than others. Fig.5.4represented XRD patterns of well crystalline B90 and BG2.

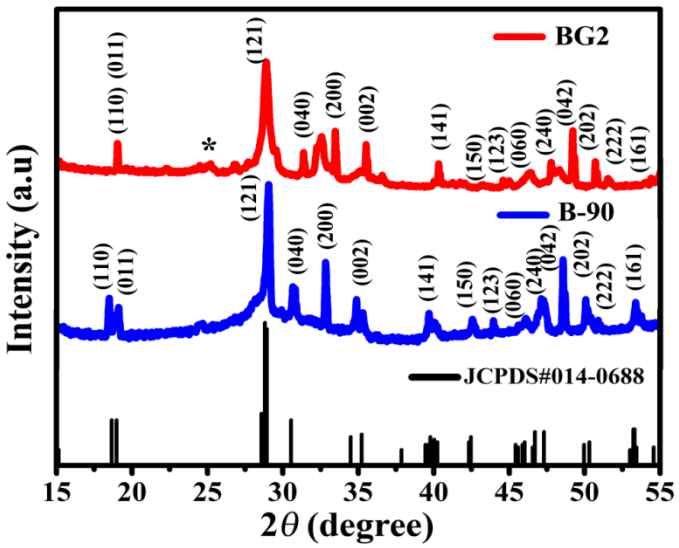

Figure 5.4: XRD patterns of $BiVO_4$ nanoparticles (B-90) and $BiVO_4$/rGO hybrids (BG2)

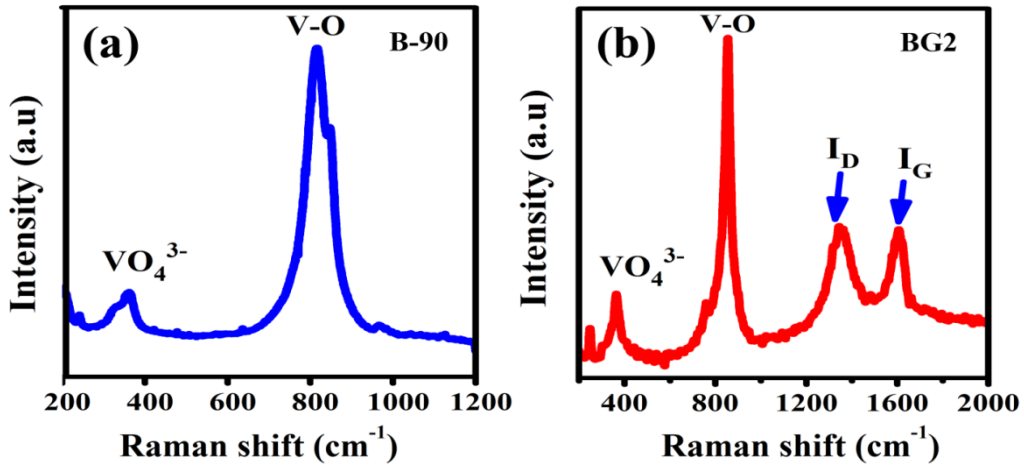

Figure 5.5: Raman spectra of B-90 and BG2.

Fig.5.5 depicts the Raman spectra of the as prepared B-90 and BG2 samples. The most intense peak at 830 cm^{-1} corresponds to the stretching modes of V-O band and the asymmetric and symmetric deformation modes of VO_4^{3-} are also present at 330 and 373 cm^{-1} respectively.[19] The bands at 1351 and 1581 cm^{-1} are assigned to D and G band of rGO also present in $BiVO_4$/rGO hybrid. The obtained D to G peak intensity ratio (I_D/I_G) is 1.16 indicating the formation of rGO in hybrid materials which also substantiates the XRD result.

X-ray photoelectron spectroscopy (XPS) has been analyzed to explicate the surface composition and chemical state of the B-90 sample. The XPS survey scan of

$BiVO_4$ indicates that the sample is consisted with Bi, V, C, and O only (Fig.5.6). The high resolution spectrum of C 1s at 284.6 eV corresponds to the adventitious carbon (Fig.5.8a) [20]. The XPS spectra of O 1s (Fig.5.8b) having two peaks at 528.5 and 531.4 eV is attributed to the lattice oxygen of $BiVO_4$ and the adsorbed H_2O or surface hydroxyl groups respectively. [21] The spin-orbit splitting of Bi 4f peaks exhibits two symmetrical peaks located at 158.2 and 163.5 eV assigning to be Bi $4f_{7/2}$ and Bi $4f_{5/2}$ respectively, confirms the Bi^{3+} state of $BiVO_4$ sample (Fig.5.8c). [21] The high resolution spectrum of V 2p (Fig.5.8d) presents two peaks at 524.8 eV (V $2p_{1/2}$) and 516.8 eV (V $2p_{3/2}$), indicating that V species exists as V^{5+} in are in $BiVO_4$. [21]

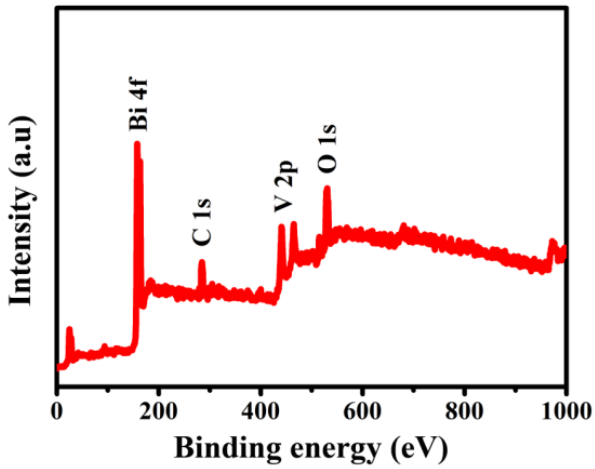

Figure 5.6: XPS survey scan of B-90 sample**.**

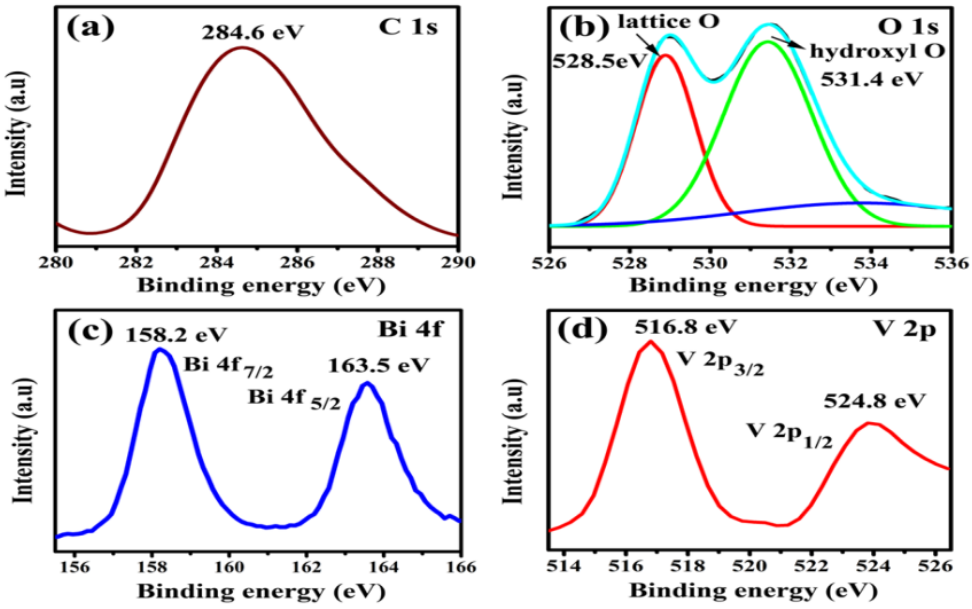

Figure 5.7:High resolution XPS spectra of (a) C 1s, (b) O 1s, (c) Bi 4f and (d) V 2P for the B-90 sample.

Fig.5.8a depicts the low magnification transmission electron microscopy (TEM) images of prepared B-90 sample. The high resolution TEM image of the sample displays the clear lattice fringe which indicates the high crystallinity of $BiVO_4$. The high resolution TEM (HRTEM) provides lattice spacing of 0.255 nm, which corresponds to the (020) lattice plane of monoclinic $BiVO_4$ (Fig.5.8b).[9] Further selected area electron diffraction (SAED) pattern consisting with bright circular spots suggests the single crystalline nature (Fig. 5.8b inset) of $BiVO_4$ sample.[22]

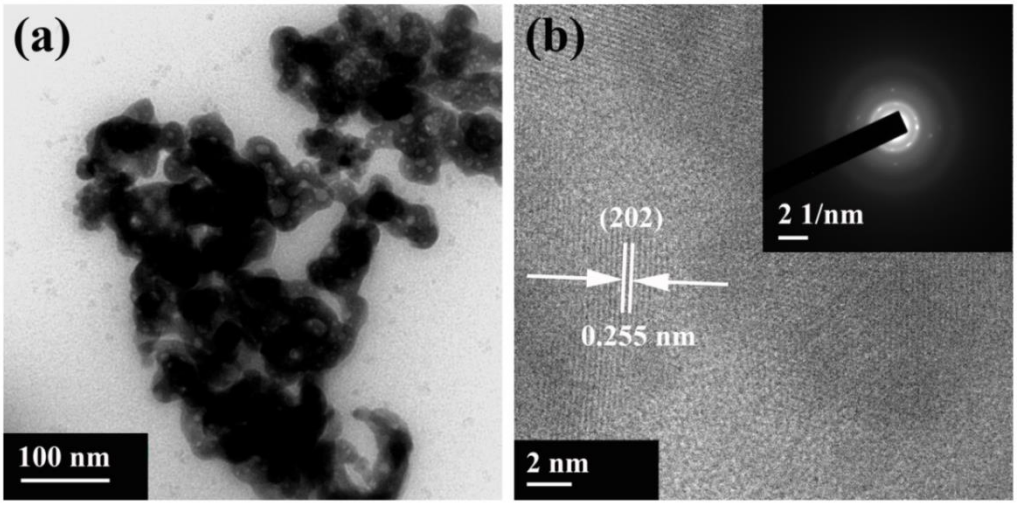

Figure 5.8: (a) Low magnification TEM and (b) HRTEM images of B-90 sample. Inset shows the SAED patterns.

5.4.2. Electrochemical study:

We have studied the cyclic voltammetry (CV) performances of the B-30, B-60, B-90 and B-120 samples at 5 mV/s scan rate in two electrode configuration using both 1M Na_2SO_4 aqueous electrolyte and PVA/H_2SO_4 gel as solid electrolyte (Fig.5.9).

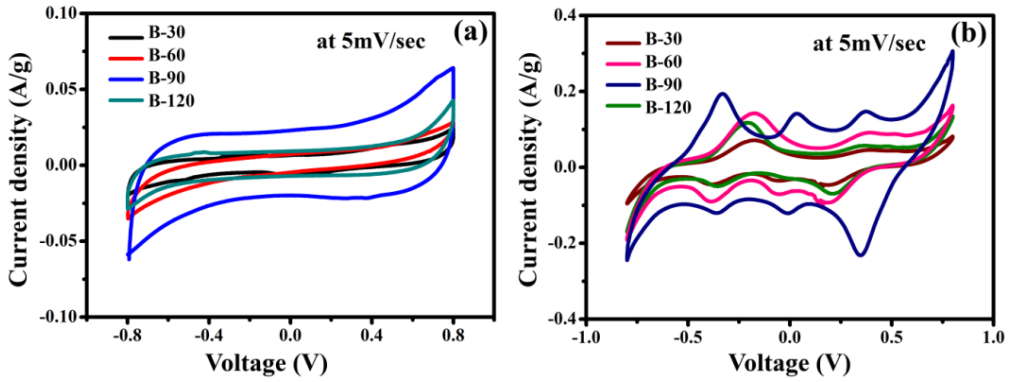

Figure 5.9: CV graphs of all $BiVO_4$ samples using both (a) 1 M Na_2SO_4 aqueous electrolyte and (b) PVA/H_2SO_4 gel electrolyte respectively.

Amongst the all samples, B-90 exhibits superior electrochemical performance due to their high surface area and well crystalline nature which is obvious from our FESEM and XRD results. Then the CV performances of all the hybrid samples BG1, BG2 and BG3 are also carried out in both the electrolytes in two electrode configurations (Fig.5.10).

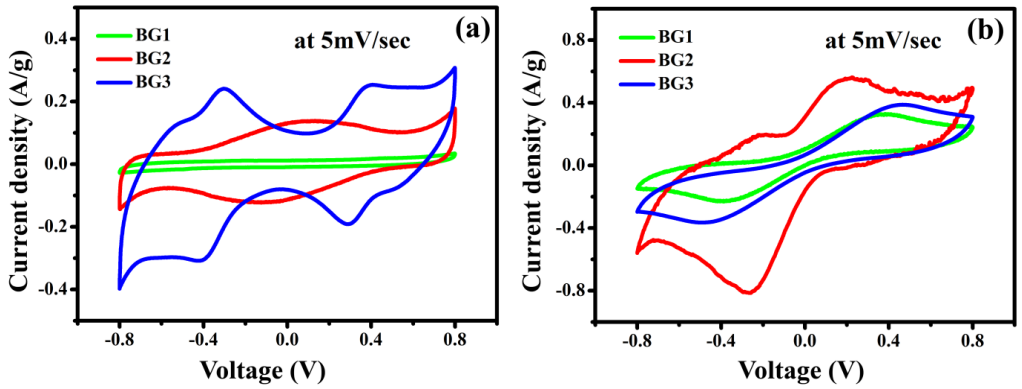

Figure 5.10: CV graphs of the $BiVO_4$/rGO hybrids using both (a) 1 M Na_2SO_4 aqueous electrolyte and (b) PVA/H_2SO_4 gel electrolyte respectively.

The enhanced electrochemical performance of $BiVO_4$/rGO hybrid electrodes over B-90 electrode can be attributed to the synergistic effect of hybrid nanostructure as in hybrids presence of rGO sheets make it more porous which ultimately promote electrolyte access and exposure of active sites to the electrolyte. Also the conducting nature of rGO widely controls the capacitive behavior of $BiVO_4$ in the hybrid electrodes providing easy access of electron transport reducing internal resistances. The specific capacitance values for all the as synthesized $BiVO_4$ and $BiVO_4$/rGO samples in two electrode configurations is displayed in Fig.5.11 and based on cyclic voltammetry performance supremacy we choose B-90 and BG2 samples for further electrochemical studies.

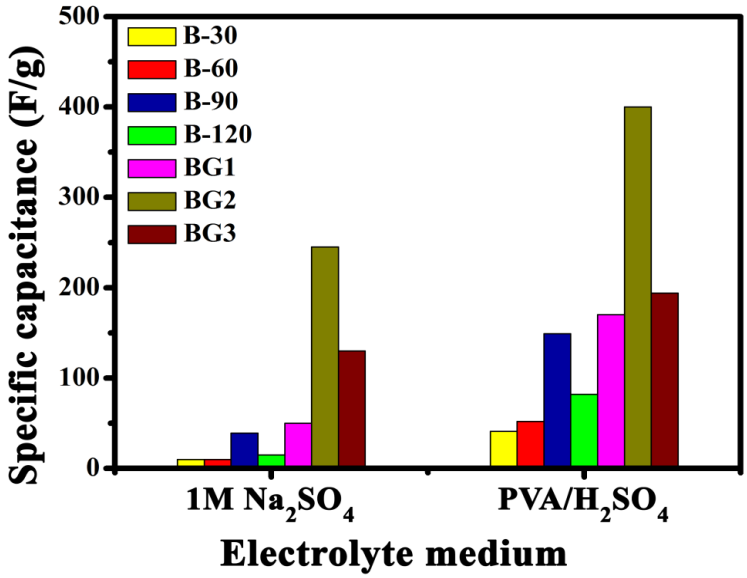

Figure 5.11: Electrochemical performance of all the $BiVO_4$ and $BiVO_4$/rGO hybrids electrodes under investigation.

Fig.5.12a represents the CV curves of the hybrid electrode (BG2) at different scan rates in solid (PVA/H_2SO_4 gel) electrolyte with a wider voltage window from -0.8 V to +0.8 V. CV curves of both B-90 and BG2 hybrid at 5 mV/s scan rate are shown in the Fig.5.12b. Well defined redox peaks are observed for CV curves of both B-90 and hybrids (BG2) at different scan rates indicating the strong pseudo-capacitive nature of electrode materials. The reversible faradic reactions occurred in the electrodes corresponding to the redox pairs V(4)/V(5) [15]. The probable reaction mechanism may be express as follows: [23]

$$BiVO_p + q\,M^+ + qe^- \leftrightarrow V_{2p-q}\,O_p M_q^{q+} \qquad \text{(Where } M^+ \text{ = Electrolyte ions)} \qquad (1)$$

The specific capacitance of hybrid electrode using PVA/H_2SO_4 solid electrolyte at different scan rate is shown in Fig.5.13c. The obtained maximum specific capacitance value is 400 F/g at 5 mV/s scan rate for the hybrid electrode materials and that for B-90 electrode materials is 149 F/g at same scan rate. The calculated specific capacitance values of the hybrid electrode are 314, 218, 119 and 58 F/g at 10, 20, 50 and 100 mV/s respectively.

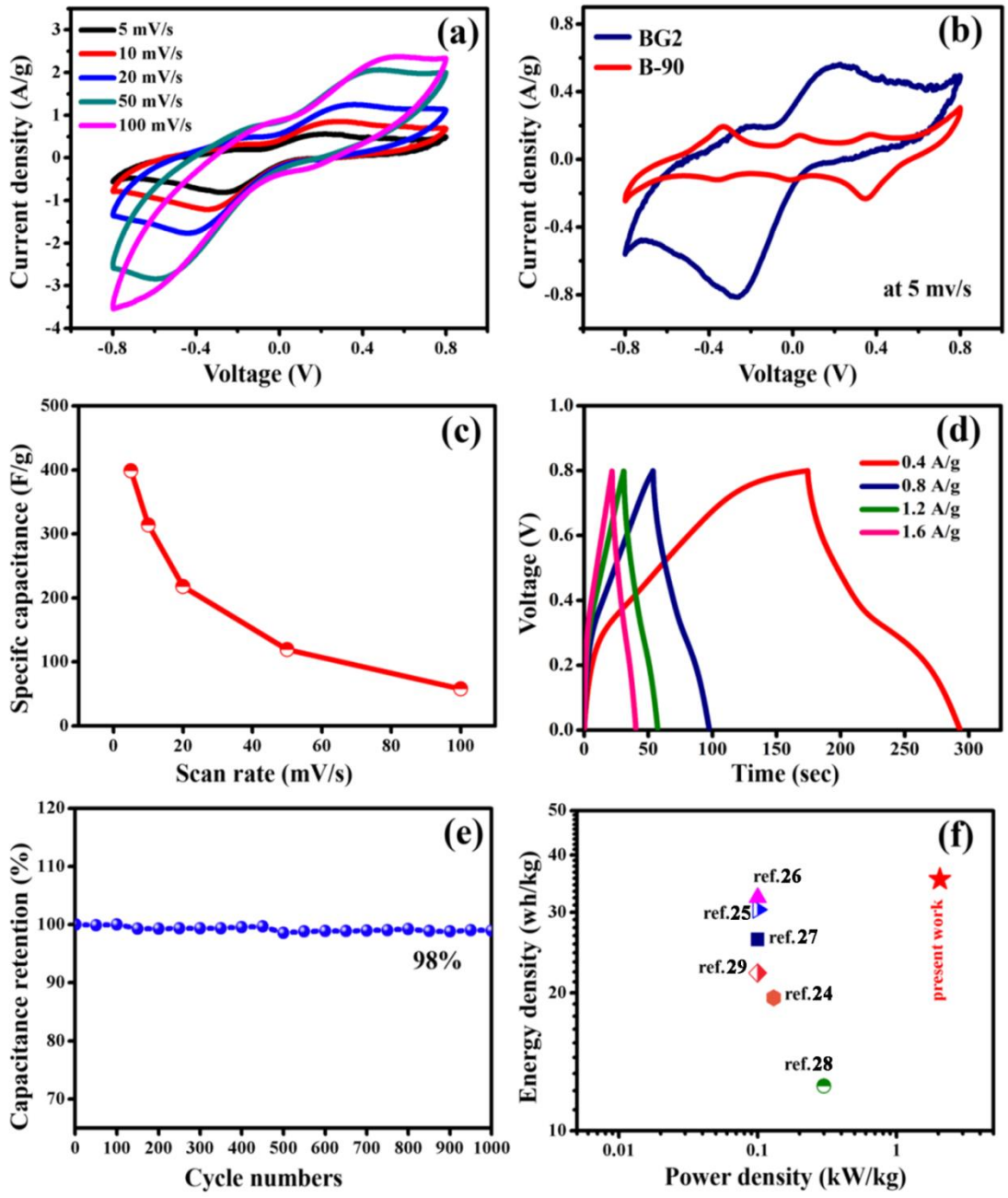

Figure 5.12: CV graph of (a) BG2 at different scan rates, (b) B-90 and BG2 at 5mV/s respectively, (c) scan rate vs specific capacitance graph of BG2, (d) galvanometric charging discharging graphs of BG2 at different current density, (e) cycle stability graph of BG2 (i) Ragone plot for $BiVO_4$/rGO hybrid (solid star) compared with the reported metal oxides.

Galvanometric charging discharging performance of the BG2 hybrid electrodes at different current density displayed typical pseudocapacitive nature and are shown in the Fig.5.12d. Cycling stability is an important parameter to determine the performance of the supercapacitor. As fabricated $BiVO_4$/rGO (BG2) symmetric supercapacitor shows

excellent stability after 1000 cycles, displays in the Fig.5.12e. The $BiVO_4$/rGO (BG2) symmetric supercapacitor retains its 98% initial capacitance after 1000 cycles. The obtained energy density for hybrid electrode is 35.37 Wh/kg at power density 2.05kW/kg. The Ragone plot of the as prepared hybrid sample and the other metal oxides based solid state supercapacitors is represented in the Fig.5.12f. The observed specific energy density is higher than the previously reported solid state supercapacitors based on metal oxides. [24-29] We have also studied the electrochemical performances of the B-90 and BG2 samples using 1M Na_2SO_4 electrolyte (Fig.5.13) by two electrode system.

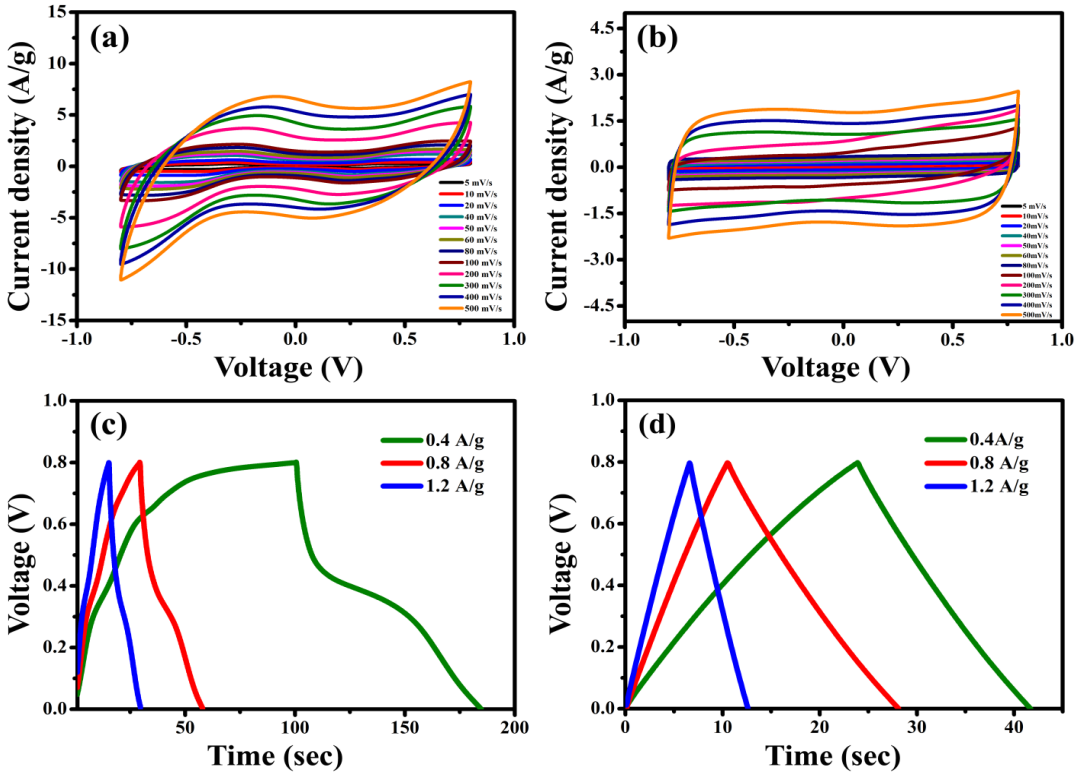

Figure 5.13: CV graphs of (a) BG2 and (b) B-90 at different scan rates and CD graphs of (c) BG-2 and (d) B-90 at different current density using 1M Na_2SO_4 electrolyte.

Fig.5.15(a) and (b) shows the cycling stability and FESEM micrographs of BG2 sample after 1000 cycle of CV execution using 1M Na_2SO_4 aqueous electrolyte exhibiting 93% of retention and durability of our sample respectively.

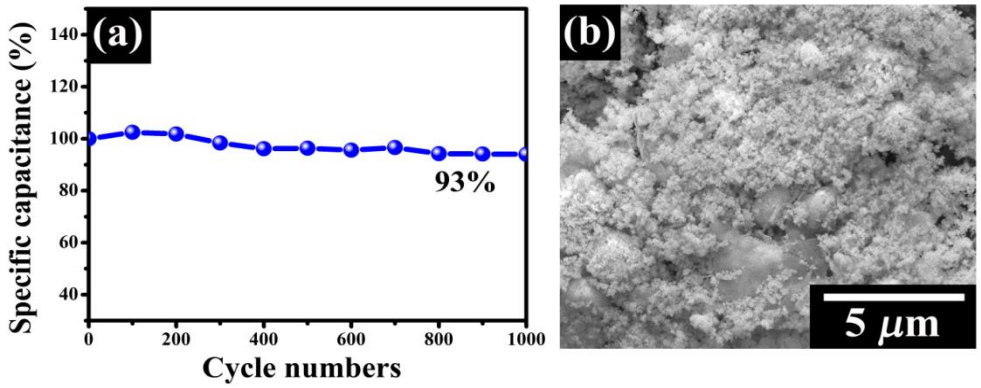

Figure 5.14: Cycling stability of BG2 for 1000 cycles at a scan rate of 100 mV s^{-1} using 1M Na_2SO_4 electrolyte, (b) FESEM image of BG2 sample after cycle test.

The non-ideal rectangular nature of the CV curves is also obtained in 1M Na_2SO_4 neutral electrolyte, which indicates the pseudo capacitive behaviors of the electrodes. The maximum specific capacitance value for BG2 electrode is 245 F/g at 5mV/s scan rate, whereas that for B-90 electrode is 39 F/g at the same scan rate. The result clearly shows better performance of the electrodes in presence of PVA/H_2SO_4 gel electrolyte. The presence of –OH groups of PVA may absorbs large water contents and enhances the ionic conductivity of the electrolyte as well as the electrochemical performances.

We have also performed the electrochemical impedance spectroscopy tests to evaluate the capacitive nature of the supercapacitors. Fig. 5.15 (a) and (b) show the Nyquist plots of the B-90 and BG2 electrodes using both 1M Na_2SO_4 and PVA/H_2SO_4 gel electrolyte over the frequency range 0.1 Hz to 0.1MHz and 0.01 Hz to 0.1MHz respectively. The equivalent series resistance values of the BG2 hybrid electrode in PVA/H_2SO_4 gel and 1M Na_2SO_4 electrolyte are obtained 2.8 and 3.8 ohm for respectively.

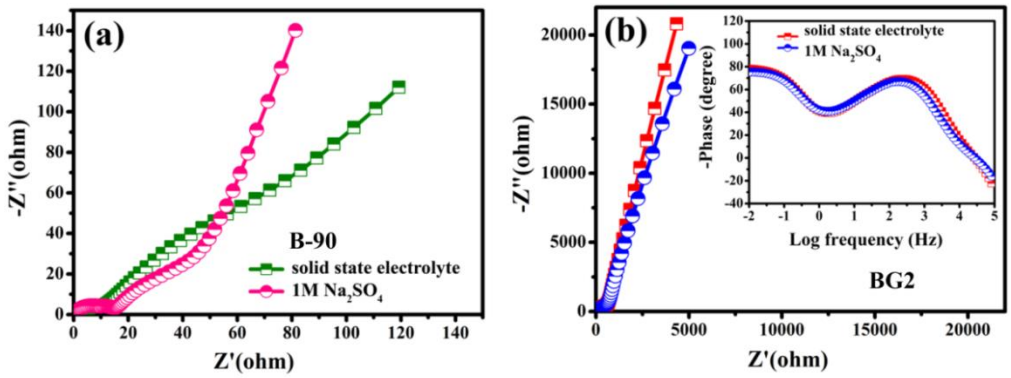

Figure 5.15: (a) Nyquist impedance plots for B-90 and (b) Nyquist impedance plots for BG2; the inset shows bode plots.

Further the straight line at low frequency region in the Nyquist plot in presence of both the electrolyte is almost parallel to the imaginary axis, which indicates the ideal capacitive performance of the supercapacitor based on BG2 hybrid electrode. The phase angle of $BiVO_4$/rGO electrodes at low frequency region for both the cases are closed to 80° (Fig.5.15b inset), which also indicates the high capacitive behavior of the electrode.

5.5 Summary

In summary, we have synthesized $BiVO_4$ embedded rGO hybrid nanostructure by a simple cost effective hydrothermal method. Structure, surface morphology and capacitive behaviors of $BiVO_4$/rGO hybrid were well investigated. X-ray diffraction pattern indicates the formation of pure phase monoclinic structure of the $BiVO_4$. We have studied the electrochemical properties of as prepared hybrid to know its performance as symmetric supercapacitor electrodes with both PVA/H_2SO_4 solid and Na_2SO_4 aqueous electrolytes. The obtained maximum specific capacitance is 400 F/g at 5 mV/s scan rate in solid electrolyte and 245 F/g in aqueous Na_2SO_4 at same scan rate. High energy density (35.37 Wh/Kg) and excellent cycle stability makes this hybrid suitable for application in supercapacitor.

5.6 References

1) S .Arico, P. Bruce, B. Scrosati, J.M. Tarascon and W.V. Schalkwijk, *Nat. Mater*., 2005, **4**, 366-377.
2) P .Simon and Y .Gogotsi , *Nat. Mater*.,2008, **7**, 845-854.
3) J. W. Lang, L B.Kong, W. J.Wu, Y. C. Luo and L.Kang, *Chem. Commun.,* 2008, 4213-4215.
4) N. R. Chodankar, D. P. Dubal, G. S Gund and C.D. Lokhande, *J. Energy Chem.*,2016 **25**, 463-471.
5) H. Kim and B. N. Popov, *J. Power Sources*, 2002, **104**, 52-61.
6) H. L.Wang, H.S. Casalongue ,Y.Y. Liang and H. J. Dai, *J. Am. Chem. Soc.*, 2010, **132**, 7472-7477.
7) P. Madhusudan, J. Ran, J. Zhang, J. Yu and G. Liu, *Appl. Catal.B,* 2011, **110**, 286–295.
8) H. Jiang, H. Endo, H. Natori, M. Nagai and K. Kobayashi, *Mater. Res. Bull.*, 2009, **44**, 700-706.
9) T. Lu and B.C.H. Steele, *Solid State Ionics*, 1986, **21**, 339-342.
10) L. Zhang, D. Chen and X. Jiao, *J. Phys.Chem. B*, 2006, **110**, 2668-2673.

11) H. Liu, R. Nakamura and Y. Nakato, *J. Electrochem.Soc*, 2005, **152**, G856-G861.

12) J. B. Liu, H. Wang, S. Wang and H. Yan, *Mater. Sci. Eng.B* ,2003, **104**, 36-39.

13) A. Galembeck and O. L. Alves, *Thin Solid Films* ,2000, **365**, 90-93.

14) Z. Khan, S. Bhattu, S. Haram and D. Khushalani , *RSC Adv.*,2014, **4**, 17378–1738.

15) S.S. Patil, D.P. Dubal, V.G.Deonikar, M.S Tamboli, J.D. Ambekar , P.Gomez-Romero, S.S. Kolekar, B. B. Kale and D. R .Patil, *ACS Appl. Mater. Interfaces*, 2016, **8**, 31602–31610.

16) Y.Arora, *Sci. Rep.*,2016, **6**, 36294.

17) W. S. Hummers and R. E. Offema, *J. Am. Chem. Soc.*,1957, **208**, 1937.

18) L. Zhang, D. Chen and X. Jiao, *J. Phys. Chem. B*, 2006, **110**, 2668-2673.

19) B. Liu, Z. Li, S. Xu, X. Ren, D. Han and D. Lu, *J. Phys. Chem. Solids*, 2014, **75**, 977–983.

20) J. K. Park, K.W. Lee, J.H. Han, J. J. Kweon, D.Kim, C. E. Lee, S .Lim, G. Kim, S.J. Noh and H.S.Kim, *J. Appl. Phys.* ,2013, **114**, 214310-214310-4.

21) X .Wu, J. Zhao, S. Guo, L. Wang, W. Shi, H. Huang, Y. Liu and Z. Kang, ***Nanoscale,*** 2016 **8,** 17314-17321.

22) L. Zhang, D. Chen and X. Jiao, *J. Phys. Chem. B*, 2006, **110**, 2668-2673.

23) S.S. Patil, D.P. Dubal D, M.S. Tamboli, J.D. Ambekar , S. S. Kolekar, P. Gomez-Romero, B.B. Kale and D.R. Patil, *J. Mater.Chem. A*, 2016, **4**,7580-7584.

24) Q.T. Qu, L. Li, S. Tian, W. Guo, Y. P. Wu and R. Holze, *J. Power Sources*, 2010 ,**195** 2789-2794.

25) Z. S.Wu, W. Ren, D.W. Wang, F .Li , B. Liu and H. M .Cheng, *ACS Nano*, 2010,**4**, 5835-5842.

26) X. Zhao, L. Zhang, S. Murali, M. D. Stoller, Q. Zhang, Y.Zhu and R.S. Ruoff , *ACS Nano*, 2012, **6**, 5404-5412.

27) J. Zhang, J. H. Li and X. S. Zhao, *Energy Environ. Sci.*, 2011, **4**, 4009-4015.

28) Q. Wang, Z. Wen and J. H. Li, *Adv. Funct. Mater.*, 2006, **16**, 2141-2146.

29) Z. Lei, J. Zhang and X. S. Zhao, *J Mater.Chem.*, 2012, **22**, 153-160.